Int J Fract (2017) 204:239–244
DOI 10.1007/s10704-016-0178-7

BRIEF NOTE

Directionality of electromagnetic radiation from fractures

Avinoam Rabinovitch · Vladimir Frid · Dov Bahat

Received: 18 April 2016 / Accepted: 17 December 2016 / Published online: 4 January 2017

Abstract The directionality of electromagnetic radiation from tensile fracturing is calculated within our previously proposed model and shown to agree with experimental observations in the field. The best locations and orientations of measuring antennas are presented.

Keywords Tensile fracturing · Electromagnetic radiation

1 Introduction

The phenomenon of electromagnetic radiation (EMR) emanating from propagating fractures (FEMR) has recently been extensively referred to in the literature (See e.g. Wang et al. 2015) conceivably due to the fact that EMR from fracturing can be of great importance both for earthquake (Wang et al. 2015) and mine-collapse (See e.g. Song et al. 2016) forecasting and for deciphering geological tectonically stress directions (Krumbholz et al. 2012). Seismic (acoustic) information of calamities such as earthquakes and mine collapses appears *simultaneously* with their occurrences and not prior to them. Therefore seismic signals cannot be used as forecasts of such events. On the other hand, since FEMR is emitted already at the early stages of both earthquakes and mine collapses, that is *before the catastrophe occurs* (between hours and days previously (King 1983; Mogi 1985; Johnson et al. 1994; Leeman et al. 2014; Balasco et al. 2015), its detection can possibly provide a forewarning of their impending occurrences. The existing deterrent in using it as a forecast seems to be the difficulty to distinguish between the relevant FEMR and the electromagnetic existing background. In our former publications we have provided both experimental qualifications of the actual EMR emanated from fractures as well as a basic physical model of its origin. One of these features is the *directionality* of the FEMR, which was scarcely touched upon there. In addition to the forecast detection problem, this characteristic is the main attribute of FEMR needed when measuring tectonic lithospheric stresses. Their directions are of importance for tectonic analyses in structural geology and for geo-engineering planning.

Following its publication (Frid et al. 2003; Rabinovitch et al. 2007), our model of FEMR has found a wide acceptance (e.g. Greiling and Obermeyer 2010). However, the model did not relate to the directionality of the radiation. We have therefore decided to add here a brief exhibition of this important feature. A short presentation of our model of FEMR is initially provided

A. Rabinovitch
Physics Department, Ben-Gurion University, Beer-sheva, Israel

V. Frid (✉)
RENA, Beer-sheva, Israel
e-mail: vladifrid@gmail.com

D. Bahat
Department of Geological and Environmental Sciences, Ben-Gurion University, Beer-sheva, Israel

both for completeness; and correspondingly to make it more approachable to scientists in these fields and to avoid some misunderstandings which have already occurred. This presentation is then followed by a discussion of radiation directionality. We concentrate here on brittle tensile (and uniaxial stress) fracturing, delaying the treatment of shear cracks to future publications.

2 The FEMR model

As a crack is created in a material, the chemical bonds between atoms (ions) are severed. Each ion, on both newly created crack sides and of both charges, is hence detached from its equilibrium position, which is located at or close to the crack side. In order to regain stability, the ions oscillate with decaying amplitude around these positions. Some ions of opposite charges find themselves at a certain time on both flanks of a crack side, thus creating a surface dipole there. These oscillating surface dipoles on both crack sides constitute the EMR sources.

Figure 1 depicts our model. It portrays five stages 1–5 in fracture growth. The two solid lines (in arrow shape) describe (exaggerated) profiles of the fracture walls (Fig. 1a). Here L is the final fracture length. Stages 1–4 occur during fracture growth, where the fracture length increases up to its maximum value, while stage 5 depicts the case post fracture termination. These stages are shared in Fig. 1a, b and d. Figure 1b schematically demonstrates the changes in the surface dipoles amplitudes during the 5 stages. The solid, heavy line depicts here a profile of the upper wall of the fracture on which are drawn the dipoles amplitudes in solid thin lines, while the dotted line relates to the lower wall on which the dipoles amplitudes were not drawn, for clarity. These amplitudes cover the whole crack surface. Shown are only amplitudes at single locations A, B, C, D. These amplitudes decay with time both along the crack length from its tip and (as seen in stage 5) following crack growth termination.

Figure 1c is a schematic 3D enlargement of the surface dipoles in positions B, C, D on both crack walls of stage 4 of Fig. 1b.

Figure 1d relates the 5 stages of crack growth and dipoles development with the EMR pulse envelope structure (dot-dashed curve in Fig. 1d). The arrows 1–5 correlate to the positions on the envelope of the 5 stages. The oscillating dashed curve describes the EMR emanating by the dipoles movements, showing the changes in amplitudes. The point t_0 is the fracture initiation; T is the time period between crack initiation and its termination; The oscillation angular velocity is $w(2\pi/w$ is the oscillation period).

One could argue that due to the different times of beginning of oscillations at different parts along the propagating crack, their contributions to the total oscillating dipole is going to be modified, since different times cause different oscillating phases and different decays. In the Appendix it is shown that, at distances far from the crack itself, the modification is expressed only by a change of amplitude and an addition of a constant phase to the oscillations. At shorter distances (not treated here) a much more elaborate analysis is needed.

3 Radiation directionality

To demonstrate the directionality of the fields consider a brittle cylinder under a uniaxial stress (Fig. 2a). Above a certain stress a crack develops in its interior into two crack sides each of area $a = Lb$ each containing its oscillating dipoles.

Consider a single dipole of magnitude p_0 in the z-direction (Fig. 2b), oscillating with a single frequency ω, i.e.:

$$\boldsymbol{p} = p_0 \sin(wt)\,\hat{z}, \tag{1}$$

where $\hat{z}$ is a unit vector in the z direction. As a result of this oscillation, both a magnetic $\boldsymbol{B}$ and an electric $\boldsymbol{E}$, fields are radiated. Most of the measuring devices are located relatively far from the crack, at distances r where $r \gg \lambda$. Here λ (see below) is the wavelength of the radiation, which in our case $\lambda \leq b$, the crack width Johnson et al. (1994). Therefore, the only parts of the radiation fields presented here will be those of the far (so called wave, e.g. Lorrain and Corson (1970)) zone. Note that, since in our case dipoles are spread on all crack area and λ is of the order of the crack width, the following treatment pertains only to cases where the distance between the measuring device and the crack-source is much larger than crack dimensions.

Each crack area a contains dipoles of average density ρ per unit area, pointing in the same direction, z, which is perpendicular to the crack sides (Fig. 2a). The magnetic and electric fields radiated by them are as follows.

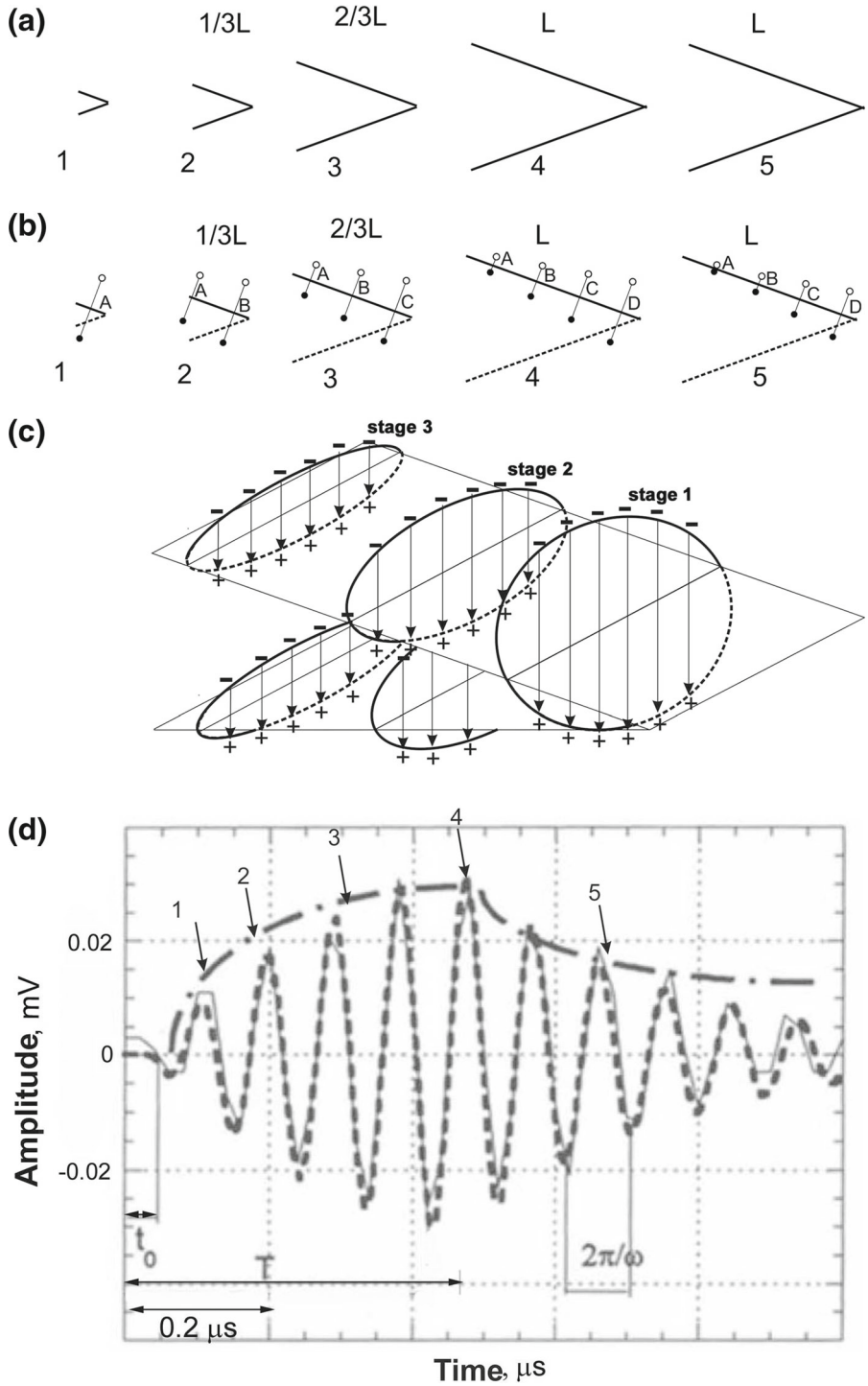

Fig. 1 Model of EMR induced by tensile fracturing of brittle materials. **a** Five stages, 1–5, in fracture growth. *Solid lines* (in *arrow* shape)—exaggerated profiles of fracture walls; L-final fracture length. Stages 1–4 occur during fracture growth; stage 5—post fracture termination case. These stages are shared in Figs. 1b and d. **b** Schematic changes in surface dipoles amplitudes during the 5 stages. The dipoles cover the whole crack surfaces. *Solid line*—profile of upper fracture wall; *Thin lines*—dipoles amplitudes at single locations A, B, C, D; *Dotted line*—profile of lower wall on which the dipoles amplitudes are not drawn, for clarity. **c** Schematic 3D enlargement of surface dipoles in positions B, C, D on both crack walls of stage 4 of Fig. 1b. **d** Locations (*arrows*) of the 5 stages of Figs. 1a–c at the EMR pulse envelope structure (*dot–dashed* curve in Fig. 1d): *Dashed curve*—EMR emanating from dipoles movements; t_0—fracture initiation time; T—period between crack initiation and termination; w—angular velocity; $2\pi/w$—oscillation period

The magnetic field $\boldsymbol{B}$ (Greiling and Obermeyer 2010) at a distance r from the crack and at an angle ϑ to the normal to the crack surface is (Fig. 2b):

$$\boldsymbol{B} = -\left[Q\rho a/r\right]\sin\vartheta\,\sin\left(wt - r/c\right)\hat{\varphi}, \tag{2}$$

where $Q = cp_0/4\pi\lambda^2$; c—the velocity of light; $\hat{\varphi}$—a unit vector in the φ direction; $w = 2\pi c/\lambda$

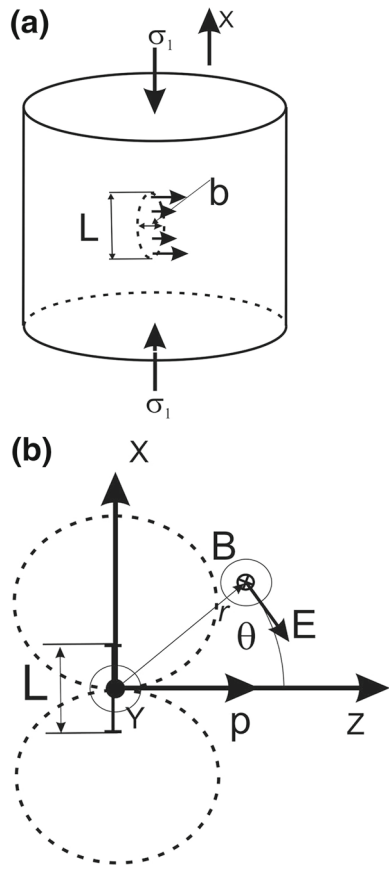

Fig. 2 EMR from tensile fracture of cylinder under uniaxial compression. **a** The cylinder under uniaxial stress, σ_1; *Dashed line*: fracture location: dimensions *Lxb*. Dipoles perpendicular to fracture surface. **b** Coordinate system (y pointing out of page) describing the directions of $\boldsymbol{E}$ and $\boldsymbol{B}$ at a distant location. Fracture in the (x, y) plane. $\boldsymbol{p}$: the combined dipole moment. *Dashed line*: the change of amplitudes of the electric and magnetic fields with $\theta(\sim \sin\theta)$. $\boldsymbol{E}$ is in the $-\hat{\theta}$ direction and $\boldsymbol{B}$ is in the $-$y direction. ⊗—the φ direction

The electric field (Lorrain and Corson 1970), $\boldsymbol{E}$, at a distance r from the crack and at an angle ϑ to the normal to the crack surface is (Fig. 2b):

$$\boldsymbol{E} = -[\mathrm{Q}_1 \rho a/r] \sin\vartheta \, \sin(wt - r/c)\, \hat{\vartheta}, \tag{3}$$

where $Q_1 = p_0/4\pi\varepsilon\lambda^2$; $\hat{\vartheta}$ is a unit vector in the ϑ direction and ε is the dielectric constant of the medium.

Either the magnetic or the electric radiation can be measured by an appropriate antenna (King 1958).

To measure the magnetic field, e.g. a loop antenna is needed. Let its area be S. The detected potential V is proportional to:

$$\oint \boldsymbol{E} \cdot \boldsymbol{dl} = -\partial/\partial t \int\int \boldsymbol{B} \cdot \boldsymbol{dS}, \tag{4}$$

where the latter integration is carried out on the antenna surface (King 1958). An additional potential can be obtained by the radiation influencing the antenna's cables (neglected here). Thus:

$$V = -[AS/r] \sin\vartheta \cos\left(wt - \frac{r}{c}\right) \cos(\hat{n} \cdot \hat{\varphi}), \tag{5}$$

where $\hat{n}$ is a unit vector perpendicular to the antenna and A is a constant.

To obtain the maximum potential by a loop antenna, it is required that: (1) The antenna be located in the plane of the crack (perpendicular to the dipoles) and (2) The normal to the loop area be in the $\hat{\varphi}$ direction (see Fig. 2b) so that the area of the antenna is perpendicular to the induced magnetic field.

To measure the electric field e.g. a line antenna is needed. Let its length be l. The detected potential V is proportional to: lE_t, where E_t is the part of the electric field tangential to the antenna. Thus:

$$V = -\left[\frac{A_1}{r} l\right] \sin\vartheta \, \sin(wt - r/c) \cos(\hat{l} \cdot \hat{\vartheta}), \tag{6}$$

where $\hat{l}$ is a unit vector in the antenna's direction and A_1 is a constant.

To obtain the maximum potential by a line antenna measuring the electric field, it is required that: (1) Again, the antenna should be located in the plane of the crack (perpendicular to the dipoles) and (2) The antenna is lying in the $\hat{\vartheta}$ (or the induced $\boldsymbol{E}$) direction (see Fig. 2b).

Stress field directions in the earth lithosphere (recent stresses) have been measured by FEMR methods (see e.g. Greiling and Obermeyer 2010; Lichtenberger 2005, 2006). For a stress causing tensional (which, under compressional load, is called extensional) fracturing, a single direction, where the detected EMR is maximal, is observed. An example to the exact measurements in a tunnel in the Upper Rhine Graben (URG) is given in (Greiling and Obermeyer 2010) and is redrawn (modified) here (Fig. 3). The recent stress direction is approximately 110°–290°.

The figure clearly demonstrates the field-amplitude dependence on $\sin\vartheta$. The principal EMR direction was identified with the maximal compression in the earth, which corresponds to $\widehat{\sigma_1}$ in Fig. 2a.

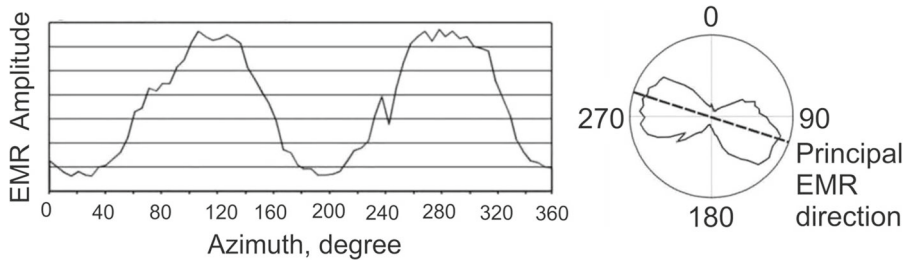

Fig. 3 (Modified Fig. 3 of Greiling and Obermeyer 2010). Experimental measurements of EMR to discover paleo-stress directions in the URG

4 Conclusion

The FEMR at distances much greater than the crack dimension is composed of oscillating electric and magnetic fields. Both fields are proportional to the second power of the frequency w and to the changing combined dipole-field amplitude which is proportional to the crack area; both decay as $1/r$ and depend on ϑ as $\sin\vartheta$ namely their maximum is located in a plane perpendicular to the dipoles or in the plane of the crack. The electric field points in the direction of $-\hat{\vartheta}$ while the magnetic field points in the direction of $-\hat{\varphi}$ (see Fig. 2b). A loop antenna should therefore be situated such that the loop plane is perpendicular to $\hat{\varphi}$ and a line antenna be situated in the $\hat{\vartheta}$ direction. The recent-stress $\boldsymbol{\sigma}_1$, being in the crack direction, is in the $\vartheta = 90^{\circ}$ orientation.

Appendix

Let t be the time since the beginning of the crack and assume the crack propagates at a constant velocity, v. Consider the crack at time t when its length is $x = vt$. The contribution to the dipole moment, p at this time from a strip of length dx' and width b located at x' and having a dipole moment of a constant density ρ (Fig. 4) is:

$$dp = Re\{2b\rho\exp[-\mu(x-x')/\mathrm{v}] \times \exp\left[i\omega\left(x-x'\right)/v\right]\}dx' \quad (7)$$

The factor of 2 comes from the two crack sides; μ is the decaying constant (in S^{-1}) and the time elapsed between its creation and the "present" is $\left(x-x'\right)/v$. The total oscillating dipole moment as seen from a distant location is the integral on x' of $dp$from $x' = 0$ to x:

$$p = Re\left\{2b\rho\exp\left(-\frac{\mu x}{v}+i\omega t\right) \times \int_0^x \exp[(\mu - i\omega)x'/v]dx'\right\} \quad (8)$$

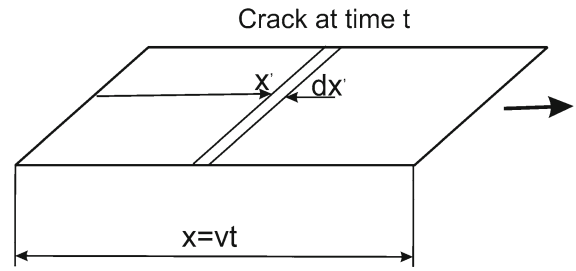

Fig. 4 Schematic one wall of the crack at time $t\,(=x/v)$ showing x and x'

Yielding

$$p = Re\left\{\frac{2b\rho v}{(\mu - i\omega}\left[1-\exp\left(-\frac{(\mu - i\omega)\,x}{v}\right)\right]\right\} \quad (9)$$

Or

$$p = Aexp\,(-\mu t)\sin(wt+\varphi)+B \quad (10)$$

where

$$A = \frac{2b\rho v}{\sqrt{(\mu^2+\omega^2}}B = \frac{2b\rho\mu v}{\mu^2+\omega^2} \quad (11)$$

And $\varphi = arctg\,(\mu/w)$.

At distances where r $\gg$ λ the only contributions to the radiation comes from$\ddot{p}$, the second time derivative of the total dipole moment. Thus B is of no consequence and the oscillation is only modified by a change of amplitude and a constant phase addition.

References

Balasco M, Lapenna V, Romano G et al (2015) The Pollino 2011–2012 seismic swarm (southern Italy): first results of the M-L=3.6 aftershock recorded by co-located electromagnetic and seismic stations. Boll Geofis Teor Appl 56(2):203–210

Frid V, Rabinovitch A, Bahat D (2003) Fracture induced electromagnetic radiation. J Phys D Appl Phys 36:1620–1628

Greiling RO, Obermeyer HJ (2010) Natural electromagnetic radiation (EMR) and its application in structural geology and neotectonics. J Geol Soc India 75:278–288

Johnson AM, Fleming RW, Cruikshank K (1994) Shear zones formed along long, straight traces of fault zones during the 28 June 1992 Landers California, earthquake. Bull Seismol Soc Am 84:499–510

King RWP (1958) Handbuch der physik, vol XVI. Springer, Goetingen

King CY (1983) Electromagnetic emission before earthquake. Nature 301:377

Krumbholz M, Bock M, Burchart S, Kelka U, Volbrecht A (2012) A critical discussion of the electromagnetic radiation (EMR) method to determine stress orientations within the crust. Solid Earth 3:401–414

Leeman JR, Scuderi MM, Marone C et al (2014) On the origin and evolution of electrical signals during frictional stick slip in sheared granular material. J Geophys Res-Solid Earth 119(5):4253–4268

Lichtenberger MJ (2005) Regional stress field as determined from electromagnetic radiation in a tunnel. J Struct Geol 27:2150–2158

Lichtenberger MJ (2006) Underground measurements of electromagnetic radiation related to stress-induced fractures in the Odenwald Mountains (Germany). Pure Appl Geophys 163:1661–1677

Lorrain P, Corson DR (1970) Electromagnetic fields and waves, 2nd edn. W.H. Freeman and Co., San Francisco

Mogi K (1985) Earthquake prediction. Academic Press, Tokyo 382pp

Rabinovitch A, Frid V, Bahat D (2007) Surface oscillations—a possible source of fracture induced electromagnetic radiation. Tectonophysics 431:15–21

Song DZ, Wang EY, Song XY, Jin PJ, Oiu LM (2016) Changes in frequency of electromagnetic radiation from Loaded coal Rock. Rock Mech Rock Eng 49:291–302

Wang W, Shan JX, Ni ZS, Kai JT (2015) Relationship between earthquake di-latency and electric precursor phenomena. Nat Hazards 79:249–262